Efficient recovery of phosphate from simulated urine by Mg/Fe bimetallic oxide modified biochar as a potential resource

Hongbo Liu, Jinhua Shan, Zhongbing Chen, Eric Lichtfouse

▶ **To cite this version:**

Hongbo Liu, Jinhua Shan, Zhongbing Chen, Eric Lichtfouse. Efficient recovery of phosphate from simulated urine by Mg/Fe bimetallic oxide modified biochar as a potential resource. Science of the Total Environment, 2021, 784, pp.1-9. 10.1016/j.scitotenv.2021.147546 . hal-03226373

HAL Id: hal-03226373
https://hal.science/hal-03226373

Submitted on 14 May 2021

HAL is a multi-disciplinary open access archive for the deposit and dissemination of scientific research documents, whether they are published or not. The documents may come from teaching and research institutions in France or abroad, or from public or private research centers.

L'archive ouverte pluridisciplinaire **HAL**, est destinée au dépôt et à la diffusion de documents scientifiques de niveau recherche, publiés ou non, émanant des établissements d'enseignement et de recherche français ou étrangers, des laboratoires publics ou privés.

Science of the Total Environment 784 (2021) 147546
https://doi.org/10.1016/j.scitotenv.2021.147546

Efficient recovery of phosphate from simulated urine by Mg/Fe bimetallic oxide modified biochar as a potential resource

Hongbo Liu [a,*,1], Jinhua Shan [a,1], Zhongbing Chen [b], Eric Lichtfouse [c]

[a] School of Environment and Architecture, University of Shanghai for Science and Technology, 516 Jungong Road, 200093 Shanghai, China
[b] Faculty of Environmental Sciences, Czech University of Life Sciences Prague, Kamýcká 129, 16500 Prague, Czech Republic
[c] Aix-Marseille Univ, CNRS, IRD, INRA, Coll France, CEREGE, 13100 Aix en Provence, France

HIGHLIGHTS

- A new type of Mg/Fe biochar was prepared to recover phosphate from urine.
- Mg/Fe biochar has excellent and stable phosphate recovery performance, with adsorption capacity up to 206.2 mg/g.
- Four mechanisms driving phosphates adsorbed onto the Mg/Fe biochar was proposed and elucidated.
- Adsorbed phosphate could be released in the neutral water and NaOH solution as a phosphate fertilizer.

GRAPHICAL ABSTRACT

ABSTRACT

The massive use of phosphate fertilizers in agriculture is costly and induces water pollution, calling for more sustainable phosphate sources in the context of the circular economy. Here we prepared a new adsorbent based on waste straw biochar modified with the Mg/Fe bimetallic oxide, namely the Mg/Fe biochar, to recover phosphate from the simulated urine as an possible phosphate fertilizer. About 90% phosphate was recovered from the simulated urine with a wide pH range of 3.0–9.0 and a maximum adsorption capacity of 206.2 mg/g, using 1 g/L of Mg/Fe modified biochar. A pseudo second-order kinetics and Sips model were proposed to fit the experimental data well, suggesting that the adsorption was controlled by physical and chemical processes, which is driven by electrostatic attraction, intra-particle diffusion, ion exchange and surface ligand exchange. Overall, the Mg/Fe biochar is renewable and can recover more than 70% of phosphate in the simulated urine after 5 cycles of reuse, which appears as a safe and efficient adsorbent to recycle phosphate from urine.

Keywords:
Biomass utilization
Modified biochar
Phosphate recovery
Mg/Fe bimetallic oxide
Adsorption model

1. Introduction

Along with nitrogen (N) and potassium (K), phosphorus (P) is a major element of plant fertilizers ensuring worldwide food security (Krey et al., 2013). However, the massive use of phosphate fertilizers has raised environmental problems. For instance, water pollution and eutrophication problems that induces the death of aquatic species (Lin et al., 2021). Most commercial phosphate fertilizers are actually extracted from finite mining resources, which are neither environmental friendly nor economically sustainable to farmers (Mew, 2016). These issues could be solved by recycling phosphates that are abundant in wastewater and urine. Urine contains abundant nutrients, such as

* Corresponding author at: 516, Jungong Road, 200093 Shanghai, China.
E-mail address: Liuhb@usst.edu.cn (H. Liu).
[1] Hongbo Liu and Jinhua Shan contribute equally to this work.

phosphate and urea, and the concentration of phosphate is 470–1070 mg/L, higher than other phosphorus containing wastewater (Bacelo et al., 2020). The direct supply of urine as fertilizer is detrimental to plant growth due to its high nutrient content. In addition, urine is expensive to transport to agricultural land, and its composition will change with pH, time and temperature (Patel et al., 2020; Randall et al., 2016). In view of this, the recovery of nutrient in urine is a more feasible utilization measure.

The existing phosphate recovery methods from urine mainly include chemical precipitation (Hu et al., 2020), ion exchange (Juntarasakul et al., 2020), membrane separation (Noubli et al., 2019) and adsorption methods (Zhang et al., 2020b). Among them, chemical precipitation method refers to adding magnesium salt to urine obtaining struvite precipitation ($MgNH_4PO_4 \cdot 6H_2O$) under alkaline conditions, which can be used as an alternative phosphate fertilizer (Kumari et al., 2020). Electrochemical methods using magnesium, iron and other metals as sacrificial anodes have been developed (Martin et al., 2020), but are limited by the cost of magnesium salt and alkali. The traditional process of phosphate recovery by precipitation crystallization often requires pre-treatment of liquid samples to reach the appropriate ratio of nitrogen and phosphorus with proper pH conditions (Gao et al., 2018; Le et al., 2020). The adsorption process has advantages of simple operation, no additional chemical dosages and low cost of phosphate recovery (Bacelo et al., 2020). Adsorption is also particularly suited to urine treatment in some remote and undeveloped areas; however the efficiency of current available adsorbents is limited.

Biochar, a porous carbon-based material, is an adsorbent obtained by pyrolysis of biomass and used for water purification, resource recovery and soil fertilization (Li et al., 2020c; Yi et al., 2020). Materials used to prepare biochar are mostly from agricultural biomass and solid waste such as rice husk (Rizwan et al., 2020), straw (Chandra et al., 2020), municipal sludge (Ma et al., 2021) and manure (Shimabuku et al., 2016), which are abundant in source and cheap to prepare. Metal atoms are easy to form coordination complexes with phosphate ions, so as to enhance the adsorption effect of phosphate of adsorbent (Liu et al., 2018). The complexing strength of metal phosphate depends on its free binding energy and is related to metal properties (Schmidtchen, 2010). Generally, the higher the valence of metal cation and the smaller the ionic radius, the more conducive the modified biochar are to bond with phosphate ions. Biochar adsorption capacity could be improved by adding metals such as Fe, Mg, Ca, Al, La, and their oxides (Godwin et al., 2019). For instance, CaO/biochar composites were synthesized using eggshell and straw, which showed excellent adsorption capacity of phosphate in the pH range 5.0–11.0 (Liu et al., 2019). Zeeshan Ajmal prepared Fe-modified magnetic biochar from rice husk and wood with the adsorption capacity of 25–28 mg/g, which is twice that of the unmodified biochar (Ajmal et al., 2020). Lanthanum-coated sludge biochar even presents a adsorption capacity of phosphate at 93.91 mg/g (Li et al., 2020a). Wang et al. reported a biochar loaded with ultra-fine ceria nanoparticles that demonstrated rapid and effective phosphate adsorption capacity. The adsorption equilibrium could be reached within 10 min, with the maximum adsorption capacity of 77.7 mg/g (Wang et al., 2020c).

Composites made of multi-metal modified biochar as new adsorbents were investigated recently (Meili et al., 2019; Zubair et al., 2020). The preparation of multi-metal composite involves the synthesis of double layered metal hydroxides (LDHs) and double layered metal oxides (LDOs) from divalent metals and trivalent metals. The composite morphology includes a main layer composed of mixed metal hydroxides, and an intercalation layer composed of anions and water molecules, which thus displays high porosity and anion exchange capacity (Li et al., 2020b; Yang et al., 2019). For instance, the addition of Mg and Al hydroxides increased the porosity of biochar to 184.0 m^2/g and enriched surface functional groups such as metal oxides MgO, Al_2O_3, C—O, and C═O (Zhang et al., 2019). Phosphate anions can provide non-bonding electron pairs, which are easy to bond with electron deficient metal ions through orbital overlap by Lewis basicity (Wu et al., 2020). Using metal oxides to modify biochar is thus expected to enrich the single surface structure of biochar and produce functional biochar materials (Vithanage et al., 2020). To our best knowledge, the adsorption performance and recovery pathway of phosphate recovery from urine using Mg/Fe biochar has not been reported. Therefore, here we synthesized the Mg/Fe biochar from waste corn straw, and we tested this material to recover phosphate from simulated urine.

In this paper, the Mg/Fe bimetallic biochar was synthesized from waste corn straws and used to recover phosphate from the urine. A couple of batch experiments were carried out to clarify the adsorption ability and mechanism. The morphology and crystal structure of Mg/Fe biochar were characterized and the effects of critical conditions for adsorption and desorption were studied to provide a environment friendly utilization of biochar by recovery of phosphate from urine.

2. Materials and methods

2.1. Materials and chemical reagents

Waste corn straw biomass was taken from the Huifeng straw plant, Jiangsu Province, China. Before use, the straw was cut to about 100 mesh, cleaned and dried fully at 60 °C. The composition of the simulated urine was set according to components of the real urine, with total phosphorus of about 140 mg/L (Supplementary material Table S1). All reagents used in the experiments were of analytical grade.

2.2. Modification and preparation of biochar

Biochar was modified by co-pyrolysis of waste biomass and Mg/Fe salts with the following procedure. (a) Firstly, 5 g of cleaned straw was put into a beaker containing 500 mL deionized water; (b) then 15.23 g $MgCl_2 \cdot 6H_2O$ and 6.77 g $FeCl_3 \cdot 6H_2O$ were added into the beaker containing straw, and continuously stirred at 60 °C in a water bath; (c) during stirring, 0.1 M NaOH and 0.5 M $NaCO_3$ solution was slowly added until the pH of the system was 10.0, then the beaker was subject to water bath at 60 °C for 4 h; (d) the mixture was washed with deionized water repeatedly until neutral, then filtered and placed in the oven at 60 °C overnight; (e) The dried mixture was transferred into a mortar, ground thoroughly, passed through a 100-mesh screen, then inserted into a tubular resistance furnace at 600 °C for 2 h under the protection of N_2. The biochar composite prepared by the above five steps was named the Mg/Fe biochar. Similarly, under the same conditions, the original biochar prepared without step (b) was named biochar.

2.3. Batch experiments of phosphate recovery

The recovery performance of the Mg/Fe biochar for phosphate in simulated urine was studied by sequencing batch experiments. The simulated urine was diluted at different times to obtain water samples with different phosphate concentrations of experimental investigations. The effects of adsorbent dosage of 0.25–4.00 g/L, contact time of 0–24 h, initial pH of 3.0–11.0 and initial phosphorus concentration of 28.0–280.0 mg/L on phosphate recovery were explored. The specific sequencing batch experiment conditions are given in Supplementary Table S2. In short, for each batch of adsorption experiments, a certain amount of biochar and the Mg/Fe biochar were added to the centrifuge tube containing 50 mL simulated urine. Then the centrifuge tube was tightened and put into a shaking box at 25 °C for 24 h at 125 rpm. After adsorption, the sample was filtered through a 0.45 μm filter membrane. The concentration of total phosphorus in the eluate was measured by a UV visible spectro-photometer at 700 nm, and the adsorption capacity and recovery rate of phosphate were calculated according to Eqs. (1) and (2):

$$Q_e = \frac{V}{M}(C_i - C_e) \quad (1)$$

$$R_R(\%) = \frac{C_i - C_e}{C_i} \times 100 \quad (2)$$

where Q_e represents the amount of phosphorus adsorbed per unit mass of adsorbent (mg P/g); V means the volume of solution (L); M means the mass of adsorbent added (g); C_i and C_e refer to phosphorus concentration (mg P/L) at the initial and equilibrium of the solution; R_R refers to the recovery rate (%) of phosphorus.

Different concentrations of NaOH solutions (0–2.0 mol/L) were used to carry out de-sorption experiments. 0.05 g of Mg/Fe biochar was put into a 50 mL centrifuge tube with simulated urine (the concentration of total phosphorus was 140 mg/L). The beaker was sealed with a sealing film. After shaking at 25 °C for 24 h, the water sample was taken out to determine the phosphate adsorption capacity Q_e. The Mg/Fe biochar-phosphate complex was obtained by drying the solid material obtained from the filtrated mixture at 60 °C. Mg/Fe biochar-phosphate complex was added into 25 mL NaOH solution to dissolve phosphate, and the phosphate content was determined after shaking for 2 h. The desorption rate was calculated according to Eq. (3):

$$R_D(\%) = \frac{C_d \times V_d}{Q_e} \times 100 \quad (3)$$

where C_d and V_d represents the concentration of phosphorus (mg/L) and the volume of NaOH solution (L), respectively. R_D is the desorption rate (%) of phosphate.

2.4. Adsorption models

Several different adsorption models were used to study the adsorption characteristics of the Mg/Fe biochar for phosphate recovery in the simulated urine (Supplementary material Table S3). The kinetics of adsorption was investigated by different contact time of 0–24 h. The data was brought into the dynamic fitting equations to determine the fitting parameters. The water samples with different initial phosphorus concentrations of 28.0–280.0 mg/L were obtained by diluting the urine with a certain multiple to study the adsorption isotherm characteristics. The adsorption capacity of adsorbent under different initial phosphate concentrations was calculated. The adsorption isotherm model was introduced to determine the fitting parameters.

2.5. Analysis methods

The phosphate was determined by the molybdate spectrophotometry. The zero point of charge pH_{ZPC} of biochar and the Mg/Fe biochar was determined by the salt drop method. Scanning electron microscopy (SEM) from Hitachi s4800, Japan, was used to determine the morphology of biochar. The mineral composition and crystal structure of biochar and Mg/Fe biochar were determined by X-ray diffraction (XRD) from Rigaku Ultima IV, Japan. Surface functional groups of Mg/Fe biochar before and after phosphate adsorption were measured by Fourier transform infrared spectroscopy (FT-IR) at 500–4000 cm^{-1} from Bruker/tensor 27, Germany. X-ray photoelectron spectroscopy (XPS) from Thermo Scientific k-alpha, USA, was used to determine the surface elemental composition and electronic state of materials.

3. Results and discussion

3.1. Characterization of prepared bio-chars

Unmodified straw biochar and biochar modified by Mg/Fe bimetallic oxides (named the Mg/Fe biochar) were synthesized by pyrolysis at 600 °C. The morphology of unmodified biochar, the fresh preparred Mg/Fe biochar and the Mg/Fe biochar after phosphate recovery were analysed by scanning electron microscopy (Fig. 1). The surface of the unmodified biochar is rather regular with a highly porous structure that provides loading space for Mg/Fe metal oxides. In the Mg/Fe biochar, metal oxides are both on the surface of biochar and within pores, showing an irregular sheet structure. This morphology was attributed to the higher disorder degree of sheets caused by shrinkage and curling of the original metal hydroxides during pyrolysis through dehydration and dehydroxylation. After the adsorption process, large crystals appeared on the biochar surface; the roughness increased, and the original pore structure was no longer visible. Here we speculated that new phosphate crystals were formed during adsorption because it had been shown that precipitation was one of the mechanisms explaining complexation of hydrous ferrous oxides with phosphate (Smith et al., 2008).

X-Ray diffraction was further used to analyze the crystallinity and chemical composition (Fig. 2). The unmodified biochar presented peaks at 26.64° and 29.55°, typical of quartz silica coming from plant biomass; the absence of other peaks was due to the non-crystalline structure of biochar. The Mg/Fe biochar showed peaks at 36.66°, 42.89° and 62.18°, which is a typical peak of Fe_2O_3 and MgO. This finding indicated that the Mg/Fe biochar had been successfully prepared. Following adsorption of phosphate, characteristic peaks of $MgHPO_4 \cdot 7H_2O$ crystals appeared at 16.49°, 20.91° and 21.53°, and peaks of $Fe(H_2PO_4)_2$ crystals at 14.46°, 30.60° and 38.28°, thus indicating good crystallinity of the Mg/Fe biochar. Overall, microscopy and X-Ray data showed successful transformations which are in line with a process involving pore filling with Mg/Fe oxides during pyrolysis, then precipitation of phosphate crystals in the simulated urine.

3.2. Effect of adsorbent dosage and initial pH

Effect of dosage of unmodified and the modified Mg/Fe biochar on the adsorption of phosphate from simulated urine was demonstrated in (Fig. 3a,c). Results showed that the unmodified biochar had low phosphate adsorption capacity ranging from 6.7 to 22.4 mg/g, and recovery values ranging from 4.2% at 0.25 g/L to 19.0% at 4 g/L. The adsorption capacity was slightly lower than the mean value of 28.9 mg/g for the unmodified biochar, which was influenced by other substances in urine (Zhang et al., 2020a). By contrast, the Mg/Fe biochar had much higher adsorption capacity ranging from 35.0 to 190.7 mg/g, and recovery values ranging from 4.2% at 0.25 g/L to 99.8% at 4 g/L. The removal efficiency was enhanced by added more adsorbents at the earlier stages, which might be attributed to more adsorption sites on the Mg/Fe biochar surface that could be contacted with phosphate. With the increase of dosage, the number of adsorption sites exceeded the amount required for phosphate contacting. Phosphate was preferentially captured by sites with strong binding force in limited phosphate content, resulting in some sites with weak binding force turning to unsaturated state (Zou et al., 2020). The low utilization of adsorption sites resulted in the decrease of biochar adsorption capacity per unit mass (Hu et al., 2018).

The capacity of unmodified biochar was low and increased slightly with pH from 3.2 mg P/g at pH 3.0 to 21.2 mg P/g at pH 11.0 (Fig. 3b). Whereas the Mg/Fe biochar had higher adsorption capacity of about 130.0 mg P/g at pH 3.0–9.0, then decreased to about 60.0 mg P/g at pH 10.0–11.0. This result was consistent with that of Zhang et al. (2019). The adsorption capacity of phosphate was related to the form of phosphate in solution and the surface charge of biochar. In the range of pH 3.0–11.0, the forms of phosphate were $H_2PO_4^-$ and HPO_4^{2-}. When the liquid pH was less than 7.2, $H_2PO_4^-$ was the main form (Wang et al., 2020a). Due to the lower adsorption free energy, $H_2PO_4^-$ was more easily adsorbed by the Mg/Fe biochar than HPO_4^{2-}. The potential of zero point charge (pH_{ZPC}) was determined as 8.9 for unmodified biochar and 10.7 for Mg/Fe biochar (Supplementary Fig. S1). There was a predominance of positive charges below pH_{ZPC} and negative charges above pH_{ZPC}. The high adsorption of Mg/Fe biochar at pH 3.0–9.0 was thus consistent with the formation of protonated groups such as protonated hydroxyl $-OH^{2+}$, which should attract and bind to phosphate anions. Lower adsorption at pH 10.0–11.0 should result

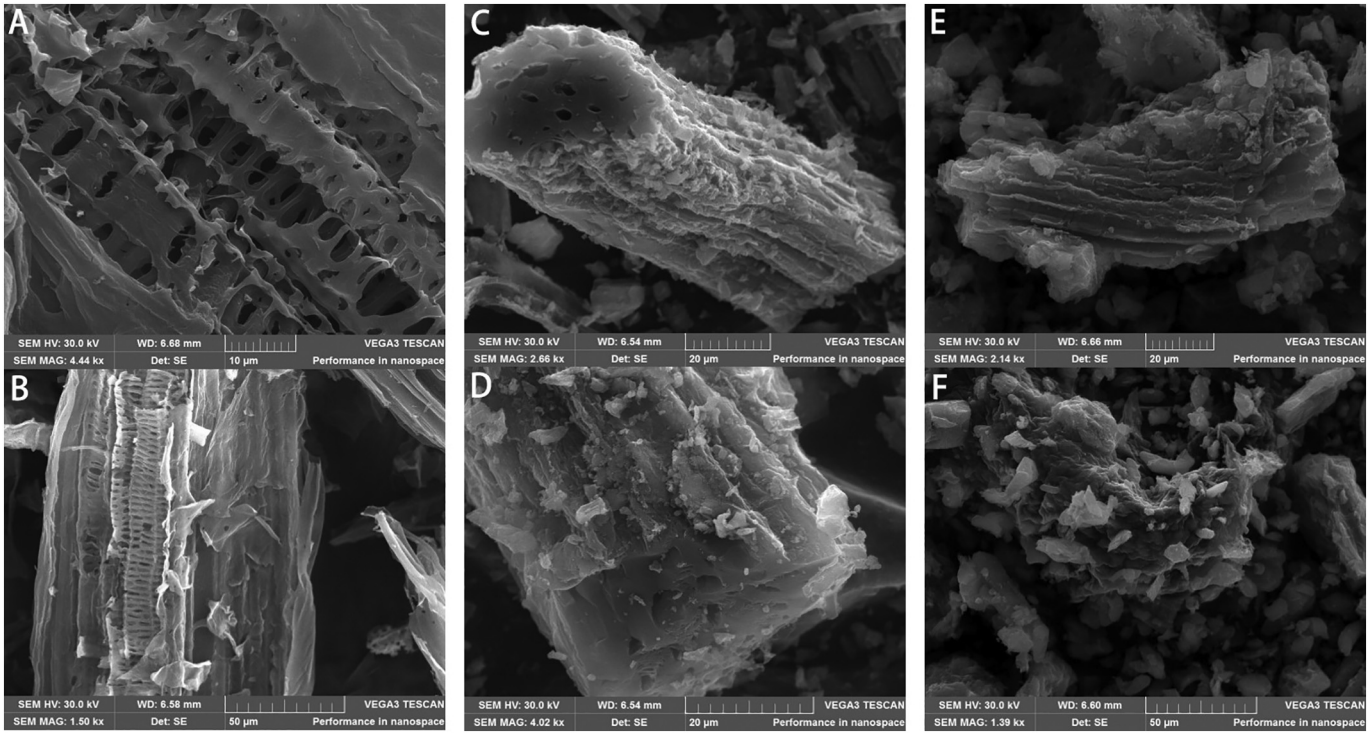

Fig. 1. SEM of the unmodified biochar (A,B), the Mg/Fe biochar (C,D) and the Mg/Fe biochar after phosphate recovery (E,F). The Mg/Fe biochar refers to biochar modified with Mg/Fe oxides.

from negative surface charges such as —O. Since the pH of urine is 6.2–9.3 (Krishnamoorthy et al., 2020), the Mg/Fe biochar was well suited to extract phosphates. Overall, our findings showed that the Mg/Fe biochar had much higher adsorption capacity than unmodified biochar; the adsorption is maximal in the urine pH range of 6.2–9.3.

3.3. Adsorption kinetics and intragranular diffusion

Adsorption kinetic data was fitted by pseudo-first-order kinetics, pseudo-second-order kinetics, and intraparticle diffusion models respectively. The parameters and fitting degree R^2 of each model were listed in Table 1 and demonstrated in Fig. 4a. Results show that the adsorption of phosphate on the Mg/Fe biochar was rapid, and more than 70% of the adsorption was completed in the first 4 h. The final recovery rate was 95.7% at 24 h. Moreover, the adsorption data fitted the pseudo-second-order kinetic model well ($R^2 = 0.990$), which was better than that of the pseudo-first-order kinetic model ($R^2 = 0.981$). It was indicated that chemical reaction was the main factor controlling adsorption (Wang et al., 2020b), which was attributed to the formation of new covalent bonds and the binding of Mg/Fe biochar surface functional groups with phosphate. Fig. 4b indicated that there were three well fitted stages in the adsorption process ($R^2 > 0.99$). The first stage of adsorption showed the rapid surface diffusion of phosphate on Mg/Fe biochar, with a high k_P value ($k_{P1} = 56.3$). At the second stage, phosphate gradually diffused to the inner pore of biochar due to the active sites on the surface of Mg/Fe biochar were gradually occupied, and the k_P value ($k_{P2} = 45.3$) in this stage was significantly lower than that in the first stage, indicating that the main factor limiting the adsorption rate was the intra-particle diffusion process. The good fitting of intra-particle diffusion model showed that the adsorption of phosphate on Mg/Fe biochar was a complex multi factor control process.

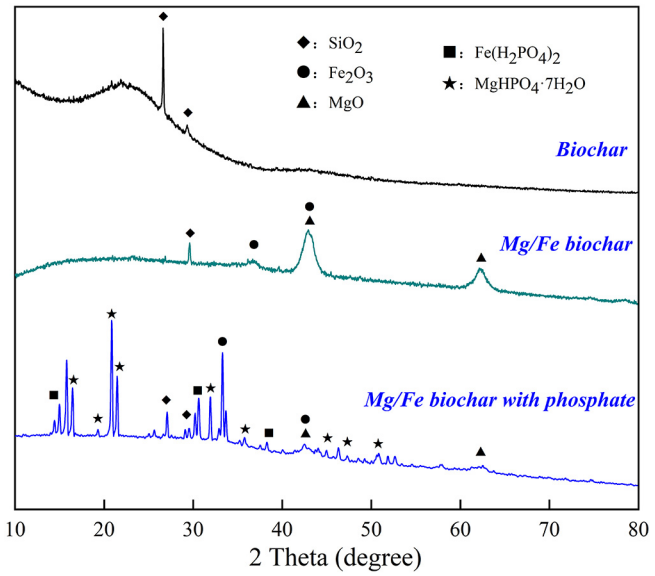

Fig. 2. X-Ray diffraction of the composite Mg/Fe biochar after phosphate recovery.

3.4. Adsorption isotherm

The adsorption isotherms of the Mg/Fe biochar for phosphate were investigated by changing the initial concentration of phosphate. The fitting curves and fitting parameters of each model were shown in Fig. 5 and Table 1, respectively. Langmuir model represents a monolayer and homogeneous adsorption process, which can determine the saturated adsorption capacity of adsorbent (Li et al., 2019). Sips model is an improvement of Langmuir and Freundlich model, which has the characteristics of both models. The adsorption data were well fitted by several models ($R^2 > 0.9$), except the Freundlich model. The Sips model provided the most accurate fitting ($R^2 = 0.971$), which suggested that the adsorption involves both physical and chemical processes. It was the same as the conclusion obtained from kinetic investigations. The maximal adsorption capacity of the Mg/Fe biochar was 206.2 mg/g by the Sips model, which is obviously superior to the

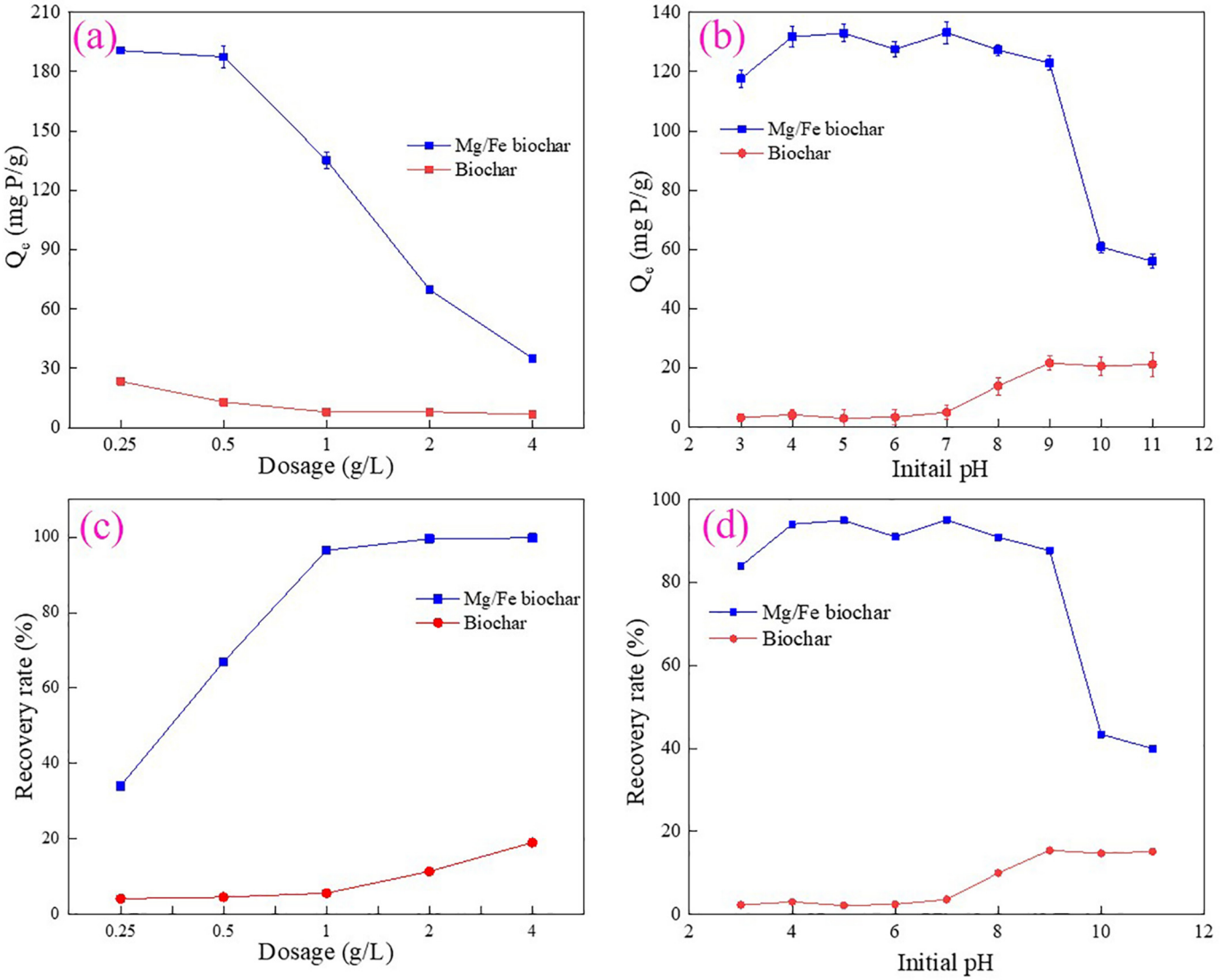

Fig. 3. Effect of biochar and the Mg/Fe biochar dosage on phosphate adsorption capacity and recovery rate (a,c); effect of initial pH on phosphate adsorption capacity and recovery rate (b, d); Qe is the amount of adsorbed phosphate, expressed in P content.

saturated adsorption capacity of biochar reported before (Supplementary material Table S4), which means that Mg/Fe biochar is a superior adsorbent for phosphate recovery in urine.

3.5. Mechanism of phosphate recovery from urine by the modified biochar

To elucidate the recovery mechanism of phosphate, surface functional groups change of the Mg/Fe biochar during the adsorption process were studied by FT-IR. The results were shown in Fig. 6a. In the infrared spectrum, the broad peak at 3438 cm^{-1} and 1618 cm^{-1} were enhanced, corresponding to the vibration of hydroxyl groups and water molecules on the Mg/Fe biochar, indicating that the hydroxyl groups and bound water increased in the adsorption reaction. In the frequency range of 1427–1402 cm^{-1}, an infrared peak corresponding to O=C–O antisymmetric stretching vibration appeared, which originated from CO_3^{2-} introduced in the preparation process of Mg/Fe biochar. After adsorption, the peak at 1427 cm^{-1} moved to near 1402 cm^{-1}, which indicated that CO_3^{2-} was involved in the adsorption of phosphate. In other studies, it was pointed out that CO_3^{2-} existed in the process of ion exchange with phosphate anion, which promoted the removal of phosphate (Jiang et al., 2021). It was noted that the peak intensities at 1090, 887 and 569 cm^{-1} were enhanced, which was attributed to the stretching of P—O bond in $HPO_4^{2-}/H_2PO_4^-$. The presence of these peaks again demonstrates the successful adsorption of phosphate (Jiang et al., 2018; Lee et al., 2019). Moreover, the representative peak of Mg—O at 670 cm^{-1} decreased after adsorption, which indicated that the Mg/Fe biochar reacted with phosphate in aqueous solution to form $MgHPO_4 \cdot xH_2O$, and was consistent with the result of XRD.

The chemical element composition and electronic state change of the Mg/Fe biochar during the phosphate adsorption process were measured by XPS analysis. Fig. 6b showed that the main components of the Mg/Fe biochar were Mg, Fe, O, and C. The photo-electron peaks with

Table 1
Calculation parameters of kinetics and isotherm model of phosphate recovery process using Mg/Fe biochar.

Models	Parameter 1	Parameter 2	Parameter 3	R^2
Pseudo-first-order	$k_1 = 0.6$	$Q_{e=}131.6$		$R^2 = 0.981$
Pseudo-second-order	$k_2 = 0.005$	$Q_{e=}150.0$		$R^2 = 0.990$
Intraparticle diffusion	$kp_1 = 53.6$	$b_1 = 0.1$		$R^2 = 0.992$
	$kp_2 = 45.3$	$b_2 = 16.8$		$R^2 = 0.999$
	$kp_3 = 0.2$	$b_3 = 134.1$		$R^2 = 0.998$
Sips	$k_S = 0.1$	$Q_m = 206.2$	$n = 0.7$	$R^2 = 0.971$
Langmuir	$k_L = 0.2$	$Q_m = 222.9$		$R^2 = 0.940$
Freundlich	$k_F = 63.3$	$n = 3.3$		$R^2 = 0.863$
Temkin	$k_T = 1.6$	a = 50.8		$R^2 = 0.936$

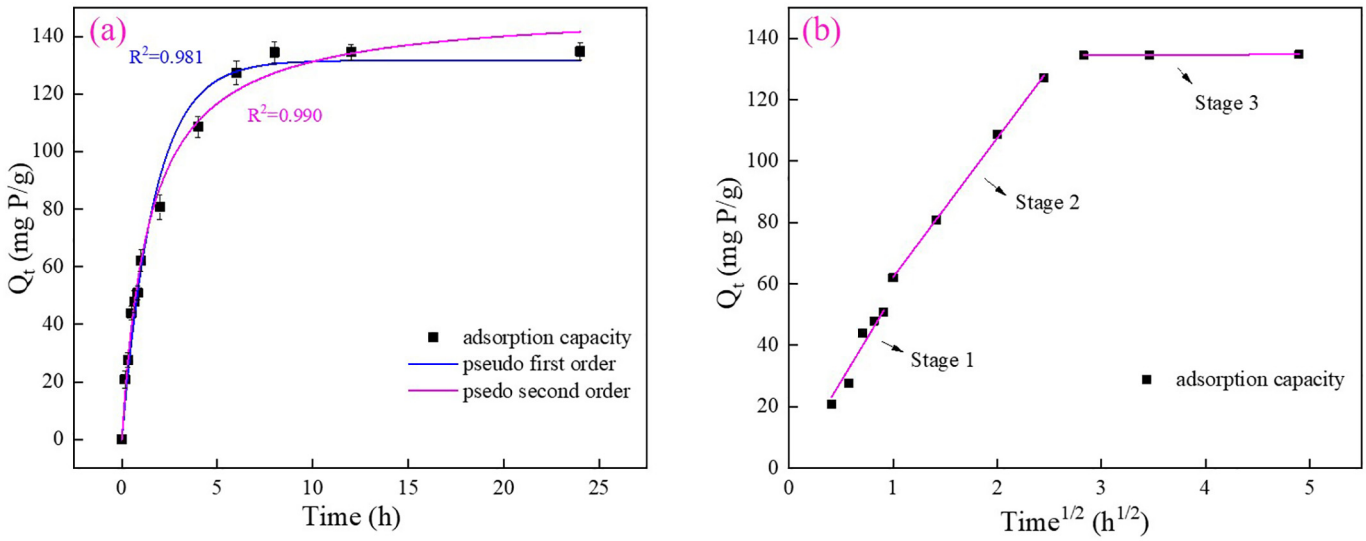

Fig. 4. Adsorption kinetics curves of the Mg/Fe biochar. The fitting line of kinetic by pseudo-first-order kinetics and pseudo-second-order kinetics (a) and intra-particle diffusion model (b) respectively.

binding energies of 1304.1, 711.0, 531.1 and 284.1 eV were attributed to Mg 1s, Fe 2p, O 1s and C 1s, respectively (Cui et al., 2019). After adsorption, a peak of P 2p was clearly observed at the binding energy of 133.1 eV, which further confirmed the successful adsorption of phosphate. The spectrum of P 2p (Fig. 6c) could be divided into three peaks of 134.7, 133.6 and 132.8 eV, corresponding to HPO_4^{2-}, metal phosphate and $H_2PO_4^-$, respectively. This indicated that phosphate could combine with metal on the Mg/Fe biochar, and the existence of interlayer phosphate anion was confirmed. Mg 1s spectra (Fig. 6d) also showed that Mg was involved in the adsorption reaction, the binding energy decreased, and the corresponding peak of metal phosphate was observed at 1303.6 and 1303.1 eV. The spectrum of O 1s (Fig. 6e) showed that before the adsorption reaction, the peak of O 1s in the Mg/Fe biochar could be decomposed into the peaks with binding energy of 529.8, 531.0 and 532.1 eV, which were attributed to M-O (M = Mg or Fe), -OH, and bound H_2O (Kong et al., 2020). After the adsorption reaction, the ratio of M-O bond decreased from 35.2% to 26.5%, while the ratio of -OH increased from 26.9% to 35.7%. This was mainly attributed to the rehydration reaction of the Mg/Fe biochar in the process of reaction. Some M-O bonds in metal oxides were converted into M-OH, which led to the increase of hydroxyl functional groups (Mallet et al., 2013). The same conclusion could be obtained from FT-IR. Fig. 6f showed the spectrum of C 1s, in which the binding energies of 284.1, 285.4 and 288.8 eV correspond to C—C, C—O and carbonate, respectively.

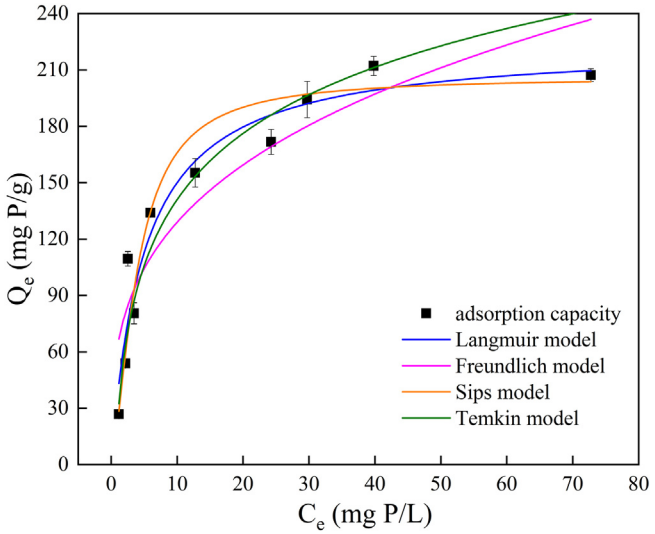

Fig. 5. Isotherm models of phosphate adsorption by Mg/Fe biochar.

The recovery mechanism of phosphate by the Mg/Fe biochar was illustrated in Fig. 7. It mainly included the following mechanisms. 1) electrostatic attraction. At low pH (less than $pH_{ZPC} = 10.7$), the hydroxyl groups on the Mg/Fe biochar surface were protonated, which had good electrostatic attraction to phosphate anions in aqueous solution. The addition of Mg/Fe oxide increased the pH_{ZPC} of the original biochar. Therefore, in a wider pH range of 3.0–9.0, Mg/Fe biochar has better adsorption capacity than the unmodified biochar. When the pH is higher than 10.0, the surface of the Mg/Fe biochar is deprotonated. Phosphate adsorption effect appears to be significantly reduced due to electrostatic repulsion (Wang et al., 2020a). 2) Intragranular diffusion. Phosphate ions were first trapped by the adsorption sites on the surface of adsorbent, and then enter the internal channels of Mg/Fe biochar through the intra particle diffusion mechanism. According to the discussion of intra-particle diffusion model, the adsorption process can be divided into three stages, in which the intra-particle diffusion stage is the main stage limiting the adsorption rate. 3) Ion exchange. In the process of Mg/Fe biochar synthesis, the conditional carbonate exchanged with phosphate in the solution, to improve the efficiency of phosphate recovery. 4) Ligand exchange. XPS analysis observed the conversion of M-O to M-OH on the surface of Mg/Fe biochar. These hydroxyl groups are replaced by phosphate groups in solution during ligand exchange. The inner-sphere complex is formed by the connection of metal atom and phosphate molecule in the form of mononuclear monodentate, mononuclear bidentate and binuclear bidentate (Wu et al., 2020). This coordination mechanism was the key for Mg/Fe biochar to recover phosphate from urine efficiently.

3.6. Desorption and cycling experiments

The regeneration ability of the Mg/Fe biochar as phosphate adsorbent and its performance after repeated use were demonstrated in Fig. 8. The desorption rate of phosphate in the Mg/Fe biochar increased with NaOH concentration, which was attributed to the electrostatic repulsion force on the Mg/Fe biochar surface and OH^- adsorption competition under high pH conditions. When the concentration of NaOH was higher than 0.5 M, the desorption rate was stable. It was noted that about 9% of the water-soluble phosphate was still released in the neutral water, indicating that the Mg/Fe biochar after phosphate recovery had the value to be used as a slow release fertilizer. 0.5 M NaOH solution

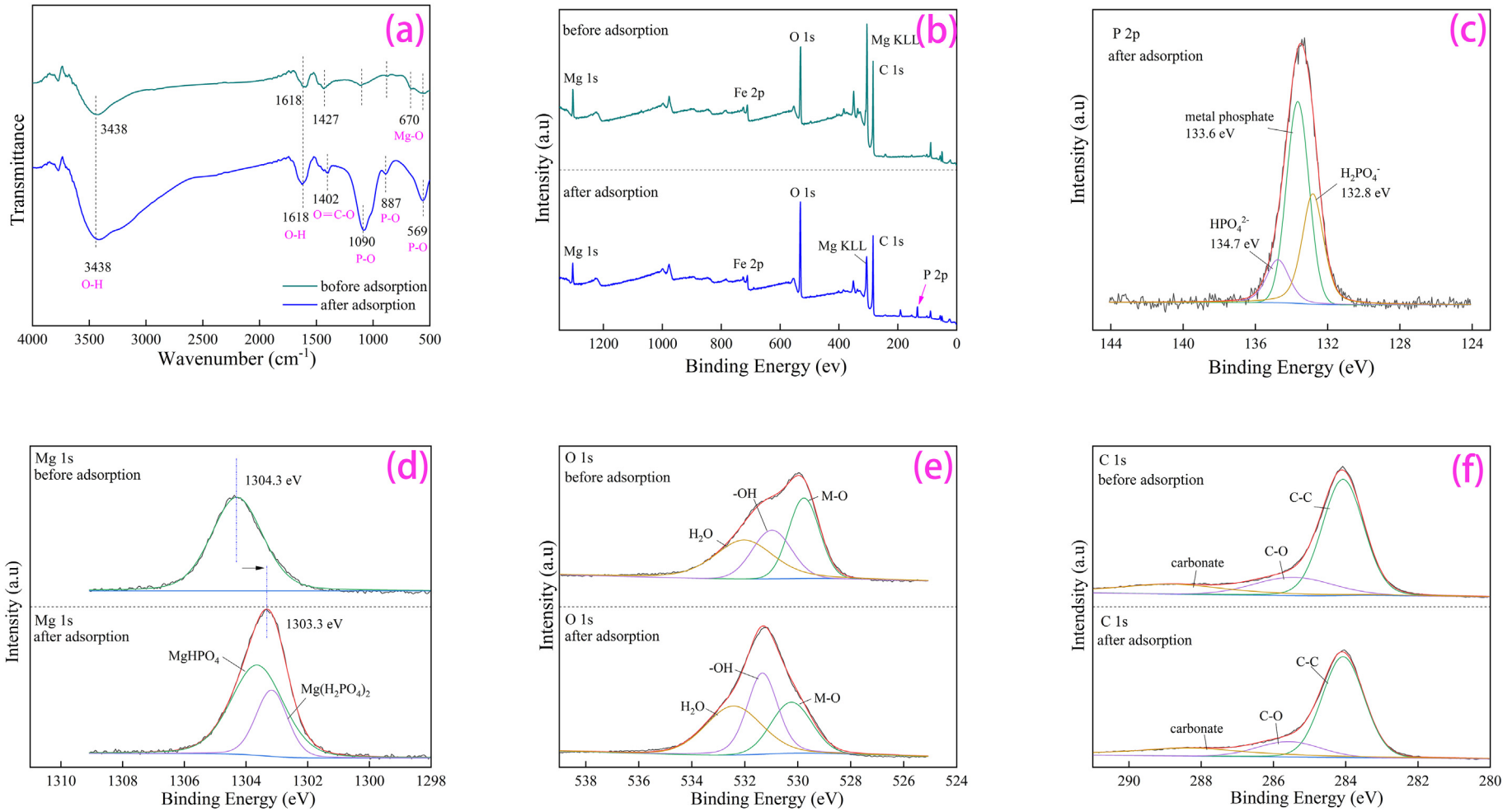

Fig. 6. FT-IR (a) and XPS analysis of Mg/Fe biochar before and after adsorption. XPS total spectra (b), P 2p (c), Mg 1s (d), O 1s (e), C 1s (f).

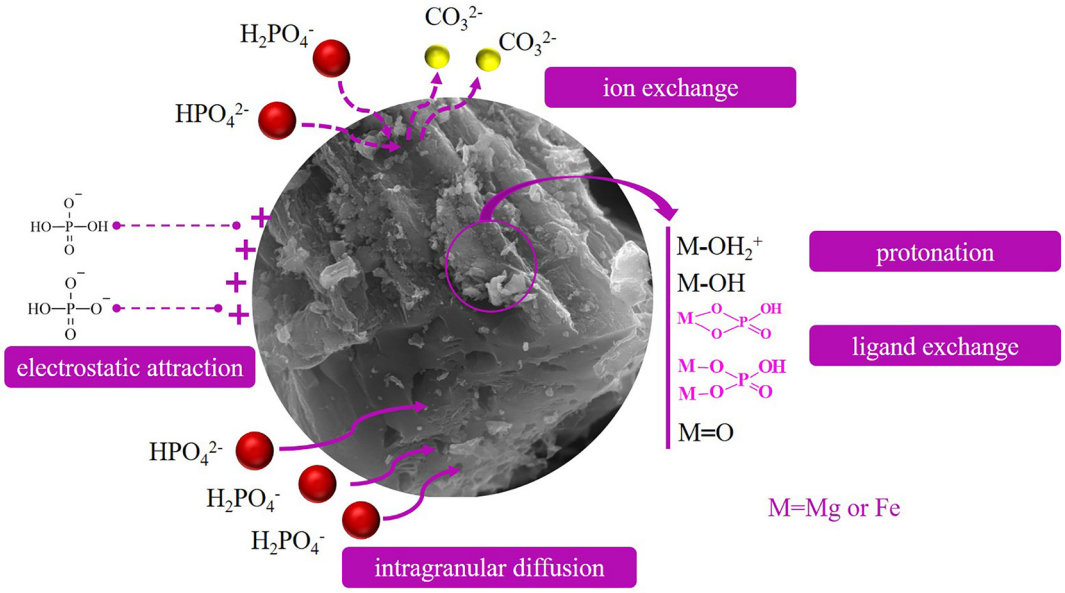

Fig. 7. Illustration of Phosphate recovery mechanism from urine with the modified Mg/Fe biochar.

was then used as desorption solution for cyclic adsorption experiments. Fig. 8b indicated that the increase in recycling times reduced the adsorption capacity of Mg/Fe biochar. After five cycles of reuse, the adsorption capacity decreased to 103.7 mg/g, and the recovery efficiency of phosphate in urine was 70.4%, which was better than other phosphate adsorption materials (Jiao et al., 2021; Luo et al., 2021). This indicated that Mg/Fe biochar could be used as an efficient adsorbent for phosphate in urine, and NaOH could be reused as eluent. Phosphate-rich eluents could be used as raw materials for commercial products such as struvite (Li et al., 2021). For some alkaline soils, the Mg/Fe biochar with phosphate could also be used as a good slow-release fertilizer and soil conditioner.

4. Conclusions

The new Mg/Fe bimetallic oxide biochar was successfully synthesized from straw and used to recover phosphate from simulated urine. More than 90% of phosphate recovery was achieved using 1 g/L Mg/Fe biochar with the urine pH range of 6.3–9.2. The maximal adsorption capacity of the Mg/Fe biochar was 206.2 mg/g, superior to the capacity of biochar reported before. The adsorption mechanism of the Mg/Fe bimetallic oxide biochar was defined as electrostatic attraction, intraparticle diffusion, ion-exchange and ligand exchange. Furthermore, the adsorbed phosphate could be released as an available fertilizer. This work provides a circular economy way to realize the recycling of agricultural waste and eutrophic sewage.

CRediT authorship contribution statement

Hongbo Liu: Conceptualization, funding acquisition, project administration, supervision, original draft.

Jinhua Shan: Methodology, lab investigation, mechanism modelling, original draft.

Zhongbing Chen: Review & editing.

Eric Lichtfouse:Review & editing.

Declaration of competing interest

This work was co-supported by the National Natural Science Foundation of China (No.52070130) and the Shuguang Project of Shanghai (Education and Scientific Research Project of Shanghai,18SG45). The authors have declared no conflict of interest.

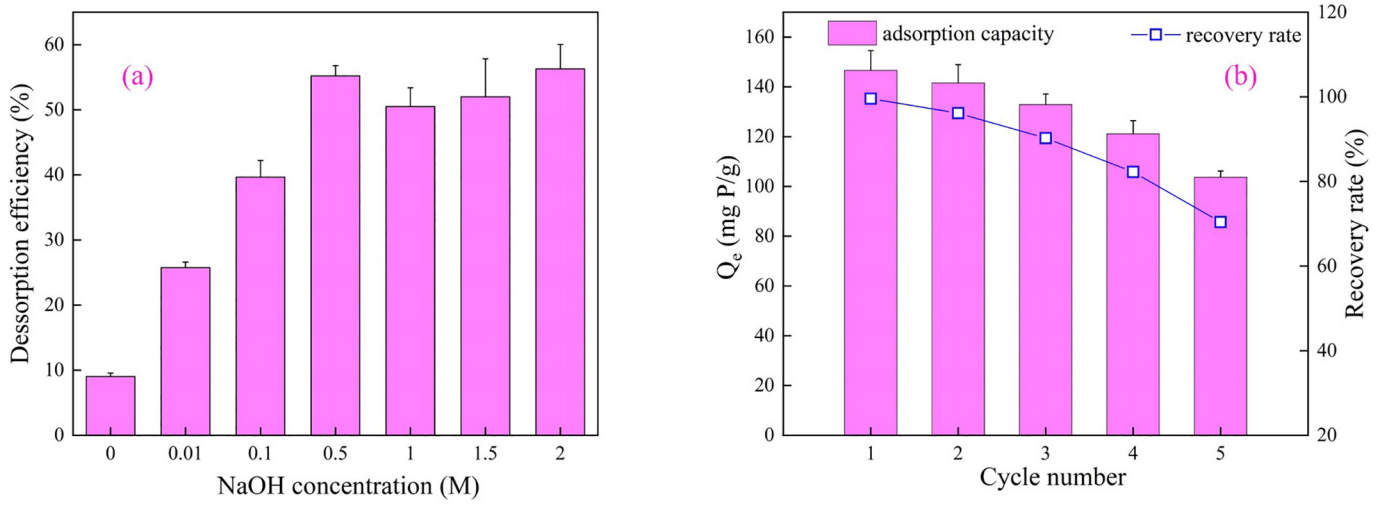

Fig. 8. Desorption performance (a) of Mg/Fe biochar in NaOH solution and cyclic adsorption performance (b).

Acknowledgments

The authors have stated that there was no conflict of interest. We gratefully acknowledged the co-funding of this work by the National Natural Science Foundation of China (No.52070130) and the Shuguang Project of Shanghai (Education and Scientific Research Project of Shanghai,18SG45).

Appendix A. Supplementary data

Supplementary data to this article can be found online at https://doi.org/10.1016/j.scitotenv.2021.147546.

References

Ajmal, Z., Muhmood, A., Dong, R., Wu, S., 2020. Probing the efficiency of magnetically modified biomass-derived biochar for effective phosphate removal. J. Environ. Manag. 253, 109730.

Bacelo, H., Pintor, A.M.A., Santos, S.C.R., Boaventura, R.A.R., Botelho, C.M.S., 2020. Performance and prospects of different adsorbents for phosphorus uptake and recovery from water. Chem. Eng. J. 381, 122566.

Chandra, S., Medha, I., Bhattacharya, J., 2020. Potassium-iron rice straw biochar composite for sorption of nitrate, phosphate, and ammonium ions in soil for timely and controlled release. Sci. Total Environ. 712, 136337.

Cui, Q., Jiao, G., Zheng, J., Wang, T., Wu, G., Li, G., 2019. Synthesis of a novel magnetic Caragana korshinskii biochar/Mg-Al layered double hydroxide composite and its strong adsorption of phosphate in aqueous solutions. RSC Adv. 9 (32), 18641–18651.

Gao, Y., Liang, B., Chen, H., Yin, P., 2018. An experimental study on the recovery of potassium (K) and phosphorous (P) from synthetic urine by crystallization of magnesium potassium phosphate. Chem. Eng. J. 337, 19–29.

Godwin, P.M., Pan, Y., Xiao, H., Afzal, M.T., 2019. Progress in preparation and application of modified biochar for improving heavy metal ion removal from wastewater. J. Bioresour. Bioprod. 4 (1), 31–42.

Hu, F., Wang, M., Peng, X., Qiu, F., Zhang, T., Dai, H., Liu, Z., Cao, Z., 2018. High-efficient adsorption of phosphates from water by hierarchical CuAl/biomass carbon fiber layered double hydroxide. Colloids Surf. A Physicochem. Eng. Asp. 555, 314–323.

Hu, L., Yu, J., Luo, H., Wang, H., Zhang, Y., 2020. Simultaneous recovery of ammonium, potassium and magnesium from produced water by struvite precipitation. Chem. Eng. J. 382.

Jiang, D., Chu, B., Amano, Y., Machida, M., 2018. Removal and recovery of phosphate from water by Mg-laden biochar: batch and column studies. Colloids Surf. A Physicochem. Eng. Asp. 558, 429–437.

Jiang, X., Zhou, D., Yan, B., Li, W., Guan, Y., 2021. Experimental and numerical investigations of phosphorus release under carbonate and variable flow in soil with Mg-Al layered double hydroxides. Chem. Eng. J. 406, 126735.

Jiao, G.-J., Ma, J., Li, Y., Jin, D., Guo, Y., Zhou, J., Sun, R., 2021. Enhanced adsorption activity for phosphate removal by functional lignin-derived carbon-based adsorbent: optimization, performance and evaluation. Sci. Total Environ. 761, 143217.

Juntarasakul, O., Yonezu, K., Kawamoto, D., Ohashi, H., Kobayashi, Y., Sugiyama, T., Watanabe, K., Yokoyama, T., 2020. Chemical state of Fe3+ in a Fe3+−type cation exchange resin for the removal and recovery of phosphate ions and the adsorption mechanism of phosphate ion to the resin. Colloids Surf. A Physicochem. Eng. Asp. 605, 125314.

Kong, L., Tian, Y., Pang, Z., Huang, X., Li, M., Li, N., Zhang, J., Zuo, W., Li, J., 2020. Needle-like Mg-La bimetal oxide nanocomposites derived from periclase and lanthanum for cost-effective phosphate and fluoride removal: characterization, performance and mechanism. Chem. Eng. J. 382.

Krey, T., Vassilev, N., Baum, C., Eichler-Löbermann, B., 2013. Effects of long-term phosphorus application and plant-growth promoting rhizobacteria on maize phosphorus nutrition under field conditions. Eur. J. Soil Biol. 55, 124–130.

Krishnamoorthy, N., Dey, B., Arunachalam, T., Paramasivan, B., 2020. Effect of storage on physicochemical characteristics of urine for phosphate and ammonium recovery as struvite. Int. Biodeterior. Biodegradation 153, 105053.

Kumari, S., Jose, S., Tyagi, M., Jagadevan, S., 2020. A holistic and sustainable approach for recovery of phosphorus via struvite crystallization from synthetic distillery wastewater. J. Clean. Prod. 254, 120037.

Le, V.-G., Vu, C.-T., Shih, Y.-J., Bui, X.-T., Liao, C.-H., Huang, Y.-H., 2020. Phosphorus and potassium recovery from human urine using a fluidized bed homogeneous crystallization (FBHC) process. Chem. Eng. J. 384, 123282.

Lee, S.Y., Choi, J.-W., Song, K.G., Choi, K., Lee, Y.J., Jung, K.-W., 2019. Adsorption and mechanistic study for phosphate removal by rice husk-derived biochar functionalized with Mg/Al-calcined layered double hydroxides via co-pyrolysis. Compos. Part B 176, 107209.

Li, J., Li, B., Huang, H., Lv, X., Zhao, N., Guo, G., Zhang, D., 2019. Removal of phosphate from aqueous solution by dolomite-modified biochar derived from urban dewatered sewage sludge. Sci. Total Environ. 687, 460–469.

Li, J., Li, B., Huang, H., Zhao, N., Zhang, M., Cao, L., 2020a. Investigation into lanthanum-coated biochar obtained from urban dewatered sewage sludge for enhanced phosphate adsorption. Sci. Total Environ. 714, 136839.

Li, S., Dong, L., Wei, Z., Sheng, G., Du, K., Hu, B., 2020b. Adsorption and mechanistic study of the invasive plant-derived biochar functionalized with CaAl-LDH for Eu(III) in water. J. Environ. Sci. 96, 127–137.

Li, X., Wang, C., Zhang, J., Liu, J., Liu, B., Chen, G., 2020c. Preparation and application of magnetic biochar in water treatment: a critical review. Sci. Total Environ. 711.

Li, X., Zhao, X., Zhou, X., Yang, B., 2021. Phosphate recovery from aqueous solution via struvite crystallization based on electrochemical-decomposition of nature magnesite. J. Clean. Prod. 292, 126039.

Lin, S.-S., Shen, S.-L., Zhou, A., Lyu, H.-M., 2021. Assessment and management of Lake eutrophication: a case study in lake Erhai, China. Sci. Total Environ. 751, 141618.

Liu, R., Chi, L., Wang, X., Sui, Y., Wang, Y., Arandiyan, H., 2018. Review of metal (hydr) oxide and other adsorptive materials for phosphate removal from water. J. Environ. Chem. Eng. 6 (4), 5269–5286.

Liu, X., Shen, F., Qi, X., 2019. Adsorption recovery of phosphate from aqueous solution by CaO-biochar composites prepared from eggshell and rice straw. Sci. Total Environ. 666, 694–702.

Luo, H., Wang, Y., Wen, X., Cheng, S., Li, J., Lin, Q., 2021. Key roles of the crystal structures of MgO-biochar nanocomposites for enhancing phosphate adsorption. Sci. Total Environ. 766, 142618.

Ma, Y., Li, M., Li, P., Yang, L., Wu, L., Gao, F., Qi, X., Zhang, Z., 2021. Hydrothermal synthesis of magnetic sludge biochar for tetracycline and ciprofloxacin adsorptive removal. Bioresour. Technol. 319, 124199.

Mallet, M., Barthelemy, K., Ruby, C., Renard, A., Naille, S., 2013. Investigation of phosphate adsorption onto ferrihydrite by X-ray photoelectron spectroscopy. J. Colloid Interface Sci. 407, 95–101.

Martin, N., Ya, V., Leewiboonsilp, N., Choo, K.-H., Noophan, P., Li, C.-W., 2020. Electrochemical crystallization for phosphate recovery from an electronic industry wastewater effluent using sacrificial iron anodes. J. Clean. Prod. 276, 124234.

Meili, L., Lins, P.V., Zanta, C.L.P.S., Soletti, J.I., Ribeiro, L.M.O., Dornelas, C.B., Silva, T.L., Vieira, M.G.A., 2019. MgAl-LDH/biochar composites for methylene blue removal by adsorption. Appl. Clay Sci. 168, 11–20.

Mew, M.C., 2016. Phosphate rock costs, prices and resources interaction. Sci. Total Environ. 542 (Pt B), 1008.

Noubli, A., Akretche, D.E., Crespo, J.G., Velizarov, S., 2019. Complementary membrane-based processes for recovery and preconcentration of phosphate from industrial wastewater. Sep. Purif. Technol. 234, 116123.

Patel, A., Mungray, A.A., Mungray, A.K., 2020. Technologies for the recovery of nutrients, water and energy from human urine: a review. Chemosphere 259, 127372.

Randall, D.G., Krähenbühl, M., Köpping, I., Larsen, T.A., Udert, K.M., 2016. A novel approach for stabilizing fresh urine by calcium hydroxide addition. Water Res. 95, 361–369.

Rizwan, M., Lin, Q., Chen, X., Li, Y., Li, G., Zhao, X., Tian, Y., 2020. Synthesis, characterization and application of magnetic and acid modified biochars following alkaline pretreatment of rice and cotton straws. Sci. Total Environ. 714, 136532.

Schmidtchen, F.P., 2010. Hosting anions. The energetic perspective. Chem. Soc. Rev. 39 (10), 3916–3935.

Shimabuku, K.K., Kearns, J.P., Martinez, J.E., Mahoney, R.B., Moreno-Vasquez, L., Summers, R.S., 2016. Biochar sorbents for sulfamethoxazole removal from surface water, stormwater, and wastewater effluent. Water Res. 96, 236–245.

Smith, S., Takacs, I., Murthy, S., Daigger, G.T., Szabo, A., 2008. Phosphate complexation model and its implications for chemical phosphorus removal. Water Environ. Res. 80 (5), 428–438.

Vithanage, M., Ashiq, A., Ramanayaka, S., Bhatnagar, A., 2020. Implications of layered double hydroxides assembled biochar composite in adsorptive removal of contaminants: current status and future perspectives. Sci. Total Environ. 737, 139718.

Wang, B., Zhang, W., Li, L., Guo, W., Xing, J., Wang, H., Hu, X., Lyu, W., Chen, R., Song, J., Chen, L., Hong, Z., 2020a. Novel talc encapsulated lanthanum alginate hydrogel for efficient phosphate adsorption and fixation. Chemosphere 256, 127124.

Wang, H., Zhao, W., Chen, Y., Li, Y., 2020b. Nickel aluminum layered double oxides modified magnetic biochar from waste corncob for efficient removal of acridine orange. Bioresour. Technol. 315, 123834.

Wang, Y., Xie, X., Chen, X., Huang, C., Yang, S., 2020c. Biochar-loaded Ce3+−enriched ultra-fine ceria nanoparticles for phosphate adsorption. J. Hazard. Mater. 396, 122626.

Wu, B., Wan, J., Zhang, Y., Pan, B., Lo, I.M.C., 2020. Selective phosphate removal from water and wastewater using sorption: process fundamentals and removal mechanisms. Environ. Sci. Technol. 54 (1), 50–66.

Yang, F., Zhang, S., Sun, Y., Tsang, D.C.W., Cheng, K., Ok, Y.S., 2019. Assembling biochar with various layered double hydroxides for enhancement of phosphorus recovery. J. Hazard. Mater. 365, 665–673.

Yi, Y., Huang, Z., Lu, B., Xian, J., Tsang, E.P., Cheng, W., Fang, J., Fang, Z., 2020. Magnetic biochar for environmental remediation: a review. Bioresour. Technol. 298, 122468.

Zhang, Z., Yan, L., Yu, H., Yan, T., Li, X., 2019. Adsorption of phosphate from aqueous solution by vegetable biochar/layered double oxides: fast removal and mechanistic studies. Bioresour. Technol. 284, 65–71.

Zhang, M., Song, G., Gelardi, D.L., Huang, L., Yong, S.O., 2020a. Evaluating biochar and its modifications for the removal of ammonium, nitrate, and phosphate in water. Water Res. 186, 116303.

Zhang, X., Shen, J., Ma, Y., Liu, L., Meng, R., Yao, J., 2020b. Highly efficient adsorption and recycle of phosphate from wastewater using flower-like layered double oxides and their potential as synergistic flame retardants. J. Colloid Interface Sci. 562, 578–588.

Zou, Y., Zhang, R., Wang, L., Xue, K., Chen, J., 2020. Strong adsorption of phosphate from aqueous solution by zirconium-loaded Ca-montmorillonite. Appl. Clay Sci. 192, 105638.

Zubair, M., Manzar, M.S., Mu'azu, N.D., Anil, I., Blaisi, N.I., Al-Harthi, M.A., 2020. Functionalized MgAl-layered hydroxide intercalated date-palm biochar for enhanced uptake of cationic dye: kinetics, isotherm and thermodynamic studies. Appl. Clay Sci. 190, 105587.

Supplementary Data

Efficient recovery of phosphate from simulated urine by Mg/Fe bimetallic oxide modified biochar as a potential resource

Hongbo Liu[1*a], Jinhua Shan[1a], Zhongbing Chen[b], Eric Lichtfouse[c]

a School of Environment and Architecture, University of Shanghai for Science and Technology, 516 Jungong Road, 200093, Shanghai, China

b Faculty of Environmental Sciences, Czech University of Life Sciences Prague, Kamýcká 129, 16500 Prague, Czech Republic

c Aix-Marseille Univ, CNRS, IRD, INRA, Coll France, CEREGE, 13100 Aix en Provence, France

Supplementary Table S1 Simulated urine formula for experiment

Reagents	Formula	Content (g/L)
ammonium chloride	NH_4Cl	0.021
potassium dihydrogen phosphate	KH_2PO_4	0.187
disodium hydrogen phosphate dodecahydrate	$Na_2HPO_4 \cdot 12H_2O$	1.155
sodium chloride	NaCl	2.500
sodium sulphate	Na_2SO_4	0.980
potassium chloride	KCl	1.146
calcium chloride	$CaCl_2$	0.075
magnesium chloride hexahydrate	$MgCl_2 \cdot 6H_2O$	0.050

Supplementary Table S2 Experimental conditions for phosphate adsorption by Mg/Fe biochar

Batch experiment	Conditions				
	Dosage (g/L)	Phosphate concentration (mg-P/L)	pH	Time (h)	Temperature (℃)
Dosage	0.25~4	140	7	24	25
Initial pH	1	140	3~11	24	25
Contact time	1	140	7	0~24	25
Initial concentration	1	28~280	7	24	25

* Corresponding author ADD: 516, Jungong Road, 200093, Shanghai, China;

Email: Liuhb@usst.edu.cn (H., Liu)

Tel: +86(21)55275979; Fax: +86(21)55275979

1 Hongbo Liu and Jinhua Shan contribute equally to this work

Supplementary Table S3 Several adsorption kinetic models and adsorption isotherm model expressions in the experiment

Models	Equations
Pseudo-first-order	$Q_t = Q_e(1 - e^{-k_1 t})$
Pseudo-second-order	$Q_t = \frac{k_2 Q_e^2 t}{1 + k_2 Q_e t}$
Intraparticle diffusion	$Q_t = k_p t^{1/2} + C$
Langmuir	$Q_e = \frac{Q_m k_L C_e}{1 + k_L C_e}$
Freundlich	$Q_e = k_F C_e^{1/n}$
Sips	$Q_e = \frac{Q_m k_S C_e^{1/n}}{1 + k_S C_e^{1/n}}$
Temkin	$Q_e = a \ln(k_T C_e)$

where Q_t and Q_e means the adsorption capacity of Mg/Fe biochar (mg/g). k_1, k_2 and k_p represent the rate constant of pseudo-first-order (1/h), pseudo-second-order (g/mg·h^{-1}) and intra-particle diffusion (mg/g·h$^{-1/2}$), respectively. Q_m represent the maximum adsorption capacity (mg/g), C_e is the phosphorus concentration at equilibrium (mg/g), k_L represent the isothermal constant (L/mg) of Langmuir model, k_F is the isothermal constant (mg/g) of Freundlich model, and k_S is the isothermal constant (L/mg) of sips model. n and a are isotherm constants. k_T is the isothermal constant of Temkin model (L/mg).

Supplementary materials Table S4 Summary of the capacity of different adsorbents to adsorb phosphate

Adsorbents	Adsorption capacity(mg/g)	References
Mg/Fe biochar	206.2	This work
La/Fe_3O_4-BC	20.5	(Wang et al., 2019)
Ce/Fe_3O_4-BC	12.5	(Wang et al., 2019)
Magnetically modified biochar (MRB/MWB)	25~28	(Ajmal et al., 2020)
GCW biochar (Mg-biochar)	63.5	(Shin et al., 2020)
$La(OH)_3$ nanorod/walnut shell biochar	75.08	(Luo et al., 2021b)
Eggshell-modified rape straw biochar	109.7	(Cao et al., 2020)
Iron-modified sludge biochar	111.0	(Yang et al., 2018)
RHB/MgAl-CLDHs	121~155	(Lee et al., 2019)
MgO/KBC	121.95	(Luo et al., 2020b)

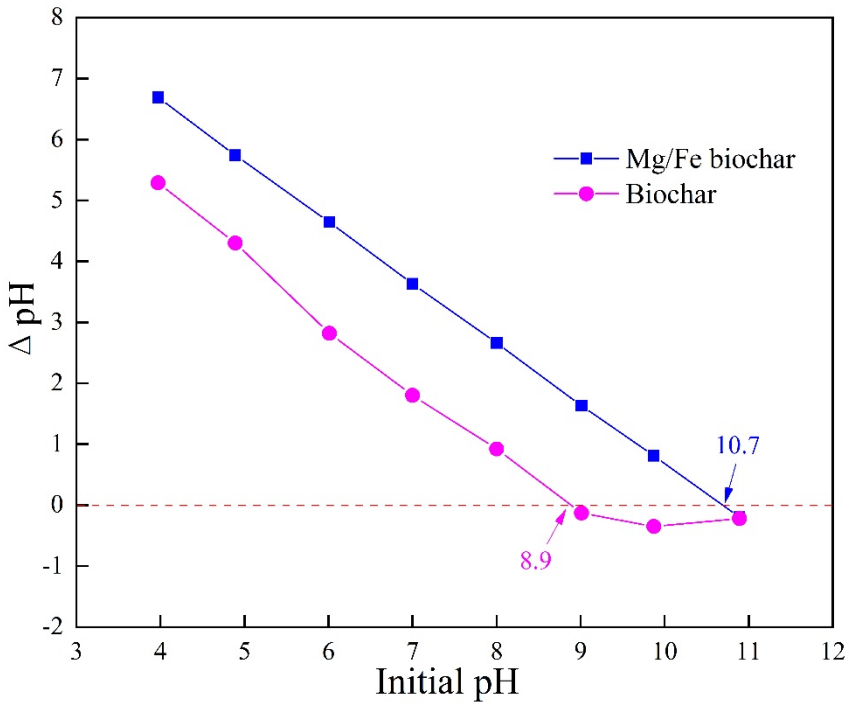

Supplementary materials Figure S1 Determination of pH_{ZPC} of biochar and Mg/Fe biochar.